Nuclear Science and Techniques (2024) 35:163
https://doi.org/10.1007/s41365-024-01511-4

Highly coupled off-resonance lattice design in diffraction-limited light sources

Yi-Hao Gong[1] · Shun-Qiang Tian[1,2] · Xin-Zhong Liu[1] · Shou-Zhi Xuan[1] · Li-Yuan Tan[2,3] · Ling-Long Mao[2,3]

Received: 7 December 2023 / Revised: 23 January 2024 / Accepted: 30 January 2024 / Published online: 6 September 2024

Abstract
The round-beam operation presents many benefits for scientific experiments regarding synchrotron radiation and the weakening influences of intra-beam scattering in diffraction-limited synchrotron light sources. A round-beam generation method based on the global setting of skew quadrupoles and the application of a non-dominated sorting genetic algorithm was proposed in this study. Two schemes, including large-emittance coupling introduced via betatron coupling and vertical dispersion, were explored in a candidate lattice for an upgrade-proposal of the Shanghai synchrotron radiation facility. Emittance variations with lattice imperfections and their influence on the beam dynamics of beam optic distortions were investigated. The results demonstrated that a precise coupling control ranging from 10 to 100% was achieved under low optical distortion, whereas full-coupling generation and its robustness were achieved by our proposed method by adjusting the skew quadrupole components located in the dispersion-free sections. The Touschek lifetime increased by a factor of 2–2.5.

Keywords Diffraction-limited storage ring (DLSR) · Shanghai synchrotron radiation facility upgrade (SSRF-U) · Round beam · Off-resonance coupling

1 Introduction

High-brightness photon beams from storage rings are critical in synchrotron radiation applications such as condensed matter material science, high-resolution imaging, medical and pharmaceutical research, and biological experiments worldwide. The fourth-generation synchrotron light sources achieve an ultra-low natural equilibrium emittance, which is a crucial parameter that determines the transverse beam dimensions and thus performance of the storage rings. MAX-IV [1] in Sweden, ESRF-EBS [2] in Europe, and SIRIUS [3] in Brazil are currently being operated with a beam emittance of 330, 135, and 250 pm·rad, respectively, and other facilities such as HEPS [4], APS-U [5], ALS-U [6], HALF [7, 8] SLS-II [9], and Elettra 2.0 [10] are in construction or approved by the government. In addition, nearly all the third-generation light sources are being explored for suitable upgrades to the X-ray diffraction limit. A small beam emittance results in a bunch of dense electrons and leads to a significant growth in emittance owing to intra-beam scattering (IBS) [11] and an apparent reduction in the Touschek lifetime [12]. Lengthening of the bunch by the harmonic cavity and round beam via the coupling effect can mitigate the IBS effect, and a round beam is preferable for a considerable number of scientific experiments [13]; therefore, the study of a potential round-beam scheme is necessary.

The round-beam scheme is achieved by exchanging the natural emittance between the horizontal and vertical planes or by generating a vertical emittance via vertical dispersion. Horizontal-field damping wigglers (HFDWs) [14, 15], Mobius accelerators [16], and the excitation and operation of linear coupling resonances [17, 18] have been proposed for the generation of round beams, as indicated in Table 1. HFDWs can increase the horizontal damping and reduce the horizontal emittance. In addition, their vertical dispersion generates a vertical emittance to achieve a round beam. The Mobius accelerator was originally proposed and tested at

✉ Shun-Qiang Tian
tiansq@sari.ac.cn

1 Shanghai Advanced Research Institute Chinese Academy of Sciences Shanghai, 201204 Shanghai, China

2 Shanghai Institute of Applied Physics Chinese Academy of Sciences Shanghai, 201800 Shanghai, China

3 University of Chinese Academy of Sciences, 100049 Beijing, China

Table 1 Techniques for the production of round beams

Technical approach	Injection	Emittance control	Optics distortion	References
Horizontal-field damping wigglers	Off-axis	Yes	Moderate	[14, 15]
Mobius accelerator	On-axis	No	Large	[16]
On coupling resonance	On-axis	No	Low	[17, 18]
Off coupling resonance	On-axis/off-axis	Yes	Large	[30]

CESR. In this type of accelerator, transverse particle coordinates are exchanged at each turn by a set of skew quadrupole magnets that equally share the natural emittance among the two transverse planes. The difference resonance operation adjusts a set of quadrupoles to match the fractional betatron tunes. The fraction of the energy of the betatron oscillation is interchanged between the transverse planes. HFDW and Mobius insertion occupy highly valuable straight sections and induce unwanted betatron functional disturbances, whereas driving the linear difference coupling resonance requires strict precision of the tune control.

In a previous method for coupling correction, a global setting of skew quadrupoles was computed with an orbit response matrix (ORM) to reduce the beam coupling and vertical beam size in a third-generation storage ring. Considering the nonlinear effect and various targets required by the high-coupling lattice design, this study proposes a round-beam generation method based on the global setting of a skew quadrupole using a non-dominated sorting genetic algorithm (NSGA-II) [19]. The precise computation of the emittances under a strong coupling was provided by the envelope method based on the equilibrium beam distribution proposed by Ohmi [20]. An accurate coupling ratio was obtained after the skew quadrupole settings were determined. However, a large betatron coupling between the two transverse directions causes difficulties in off-axis injection [21, 22], whereas a large vertical dispersion leads to extra emittances and a reduction in brightness. Attempts to generate only vertical dispersion without betatron coupling or betatron coupling without vertical dispersion have been studied.

The lattice of the SSRF-U [23] storage ring, as an update of SSRF [24–26], with a circumference of 432 m, designed having a beam energy of 3.5 GeV, and achieving a natural emittance of 72.3 pm·rad, consists of 20 seven-bend achromatic (7BA) cells forming four super-periods, whereas the lattice of SSRF [27–29] has 20 DBA cells (four folds), and the beam emittance is 3.9 nm·rad at the same beam energy. A global setting of skew quadrupoles at a reasonable magnetic strength range on the storage ring can effectively achieve a given coupling ratio, whereas the other beam parameters must meet the requirements of beam stability. Achieving the least number of side effects on a strongly coupled lattice is desired.

Section 2 presents the methodology of NSGA-II and the coupling computation. Section 3 presents the achievement of a precise coupling control with low beta-beating by using the envelope method and NSGA-II. A round-beam scheme generated almost completely via betatron coupling is presented in Sect. 4. The nonlinearity effect on the dynamic aperture, optimization of the energy acceptance, and computational results of the beam lifetime are presented in Sect. 5. Finally, the conclusions are presented in Sect. 6.

2 Achieving large coupling via the optimization algorithm and coupling computation

To obtain a large coupling ratio or round beam in a storage ring, the linear lattice design can be summarized as an optimization problem [30] by assigning the magnet with a skew component and the other magnets to simultaneously optimize the following factors: (1) ϵ_{I}, ϵ_{II}, which are the eigenemittances of mode I and II, to guarantee the required brightness, and $|\frac{\epsilon_{\mathrm{II}}}{\epsilon_{\mathrm{I}}} - C|$ to achieve the target coupling ratio C. (2) RMS beta-beating from the original uncoupled lattice to ensure the existence of stable linear solutions. (3) The fractional tune is sufficiently distant from the low-order resonances and other nonlinear effects. Skew quadrupole components that directly affect the coupling, emittance, and linear optics were applied to solve the optimization problem under these constraints.

2.1 Coupling computation

To achieve a strong coupling control, a precise computation and measurement of the coupling ratio are required. Beam emittances with linear coupling can be analyzed using perturbation theories. The coupling measurement considers the closest tune distance during tune-crossing predicted by the linear coupling resonances as the magnitude of the coupling coefficient κ, as an important coupling measure method, and the coupling ratio is therefore $\frac{\epsilon_y}{\epsilon_x} = \frac{\kappa^2}{\Delta_r^2+\kappa^2}$, where $\Delta_r = \nu_{0x} - \nu_{0y} - l$. However, when the linear coupling is sufficiently strong, these analyses of the beam parameters may not be accurate, and the envelope method based on the equilibrium beam distribution [31] provides accurate results for the emittances, despite the presence of a strong coupling. The equilibrium beam distribution is obtained via particle tracking considering radiation damping and quantum excitation as follows:

$$\Sigma = \begin{pmatrix} \langle x^2 \rangle & \langle xp_x \rangle & \langle xy \rangle & \langle xp_y \rangle & \langle xz \rangle & \langle x\delta \rangle \\ \langle p_x x \rangle & \langle p_x^2 \rangle & \langle p_x y \rangle & \langle p_x p_y \rangle & \langle p_x z \rangle & \langle p_x \delta \rangle \\ \langle yx \rangle & \langle yp_x \rangle & \langle y^2 \rangle & \langle yp_y \rangle & \langle yz \rangle & \langle y\delta \rangle \\ \langle p_y x \rangle & \langle p_y p_x \rangle & \langle p_y y \rangle & \langle p_y^2 \rangle & \langle p_y z \rangle & \langle p_y \delta \rangle \\ \langle zx \rangle & \langle zp_x \rangle & \langle zy \rangle & \langle zp_y \rangle & \langle z^2 \rangle & \langle z\delta \rangle \\ \langle \delta x \rangle & \langle \delta p_x \rangle & \langle \delta y \rangle & \langle \delta p_y \rangle & \langle \delta z \rangle & \langle \delta^2 \rangle \end{pmatrix} \tag{1}$$

The horizontal and vertical emittances, local beam tilt, and beam size were determined once the six-dimensional distribution matrix Σ was calculated. The anti-symmetric matrix S is defined as follows:

$$S = \begin{pmatrix} 0 & 1 & 0 & 0 & 0 & 0 \\ -1 & 0 & 0 & 0 & 0 & 0 \\ 0 & 0 & 0 & 1 & 0 & 0 \\ 0 & 0 & -1 & 0 & 0 & 0 \\ 0 & 0 & 0 & 0 & 0 & 1 \\ 0 & 0 & 0 & 0 & -1 & 0 \end{pmatrix} \tag{2}$$

The eigenvalues of ΣS are $\pm i\varepsilon_k$, where ε_k indicates the equilibrium emittance of modes I, II, and III. The rotation of the phase space in the horizontal, vertical, and longitudinal planes provides the orientation of the normal modes compared with the axes of the physical system. Thus, modes I, II, III are defined as the eigenmode motions in the "eigendirections". In the simulation, the envelope matrix is computed by using the *Accelerator Toolbox* [32] function *ohmienvelope* developed by the formalism proposed by Ohmi, Hirata, and Oide and the *Elegant* function *moment_out* [33]. Referring to SSRF-U as the update of SSRF, a feasible and cost-effective plan is to employ skew quadrupole components induced by winding on a sextupole magnet. A total of 120 sextupole magnets of SSRF-U were grouped into families for chromaticity correction, with six sextupoles installed in each 7BA cell. Thus, the beam coupling was adjusted by manipulating 120 sextupole winding skew quadrupoles and then determining the corresponding accurate coupling ratio using the envelope method. Meanwhile, all chromaticity correction sextupoles were located in the dispersive region; therefore, these skew quadrupoles generated a significant vertical dispersion and strong betatron coupling, leading to a growth in emittances in mode II.

2.2 NSGA-II algorithm and objective functions

Genetic algorithms have been widely demonstrated to be useful techniques in many optimization problems of accelerators, especially those that are complex, such as nonlinear optimization [33, 34]. NSGA-II is an evolutionary algorithm used for multi-objective optimization problems that can be applied to our study. It ranks solutions based on their non-dominated status using the Pareto dominance. It incorporates elitism to preserve the best solutions, uses genetic operators for exploration and exploitation, and maintains diversity along the Pareto front. NSGA-II converges toward the true Pareto front, providing decision-makers with a range of trade-off options. There are six sextupoles in each cell of the SSRF-U lattice, as shown in Fig. 1. A total of 120 independent skew quadrupole components coiling on two families of sextupoles in the dispersive region with a limitation of the magnet strength can be selected as a set of variables devoted to coupling control in a minimization algorithm.

Because the goal of coupling control is apparently the coupling ratio standing the ratio of the vertical and horizontal emittances, the achievement of the eigenemittance coupling ratio defined by $\varepsilon_{II}/\varepsilon_{I}$ is a simple task under global skew quadrupole settings, whereas the arbitrary change of skew quadrupoles can severely affect the beam parameters,

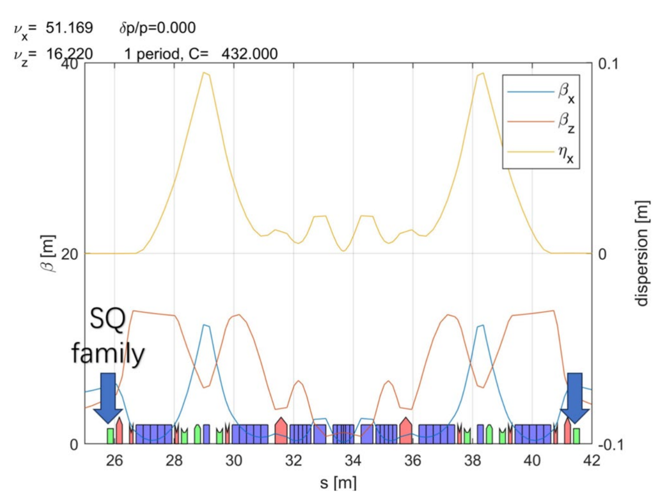

Fig. 1 (Color online) Linear optics and structures of one SSRF-U storage ring lattice cell; the blue rows indicate the skew quadrupole (SQ) families in the dispersion-free region

such as beam optics, especially at a large coupling. Therefore, we considered the coupling ratio as a constraint, where the computed coupling ratio was close to the target coupling ratio; otherwise, the set of skew quadrupole components was considered invalid. Both eigenemittances, ε_{I} and $\varepsilon_{\mathrm{II}}$, as well as the RMS beta-beating computed via the parameterization proposed by Edwards and Teng (ET) [36], were considered as the optimization objectives in NSGA-II. The constrained condition is defined as the difference between the expected and calculated coupling ratios, and the vector space for searching for the best solution is a two-dimensional vector of skew quadrupole strengths. Each solution in the population is considered a child in the parameter space. In NSGA-II, we initialized a population of solutions, selected parents via a binary tournament, and then generated a child-simulated binary crossover (SBX). After non-dominated sorting, the best solutions were selected, and the features were inherited by the next generation. The crowding distance was used to maintain the diversity of the best solutions in the objective space.

3 Low betatron coupling with skew quadrupoles in dispersive region

3.1 Skew quadrupoles setting with optimization algorithm

A population of 100 children and 100 iterations was initialized for the optimization until the convergence was satisfactory, and a set of optimal configurations was obtained. A $5-20\%$ target coupling ratio was used to test the reliability and fit various requirements for future lattice designs. To consider the lattice symmetry, two families of skew quadrupoles applied with their respective strengths were chosen to feed into the optimization algorithm. The strength of the normalized skew quadrupoles was limited to less than $0.1\,\mathrm{m}^{-2}$.

The results of the calculation are shown in Table 2. A good agreement was achieved between the setting of the beam coupling and optimal results under a significantly low RMS beta-beating in both the horizontal and vertical directions to maintain a stable linear solution, indicating that

Table 2 Optimization results of the NSGA-II algorithm for each emittance coupling ratio setting, calculated coupling ratio, calculated vertical emittances, and RMS beta-beating

Set $\varepsilon_y/\varepsilon_x$	$\varepsilon_{\mathrm{II}}/\varepsilon_{\mathrm{I}}$	$\varepsilon_{\mathrm{II}}$ (pm · rad)	β_x/β_y beating
0.05	0.051	3.65	0.6%/0.5%
0.10	0.098	7.24	1.3%/0.7%
0.20	0.205	14.52	5.6%/1.7%

we can achieve a large beam coupling without additional quadrupole adjustments for beam optics correction. Meanwhile, the total emittance of the beam increasing owing to the larger beam coupling can be interpreted as the vertical dispersion generated in the dispersion area. Therefore, if full coupling is required, additional large emittances nearly double the total emittances are unacceptable. A significantly fast convergence was also observed during the optimization; the best solution was obtained in a few iterations. Because the fractional tune changes owing to the optical distortion and can be corrected to the original tune by tuning the correction quadrupoles, tuning can avoid the difference in resonance, and the closed orbit distortions can be corrected owing to the unnoticeably sensitive coupled lattice.

3.2 Equilibrium emittances based on the tracking, global beam size, and effective emittances

The skew quadrupoles setting of the 10% coupling was examined by tracking using the *Elegant* code. A total of 5000 particles were tracked with 20,000 turns with synchrotron radiation and quantum excitation. The tracking results from *Elegant* demonstrate that both transverse beam distributions reach equilibrium, and the horizontal and vertical emittances remain stable around the emittances predicted ($\varepsilon_x = 72.5\,\mathrm{pm}\cdot\mathrm{rad}, \varepsilon_y = 7.3\,\mathrm{pm}\cdot\mathrm{rad}$) with the aforementioned computations after 10,000 turns with no particle loss.

The beam size can be determined both by the computed beam envelope or by the Sands formalism [37] using the ET parameterization. Considering the given equilibrium emittances and energy spread, the beam size along the ring can be computed using the formula given by the linear coupled analysis [38] and proven in [30]. Here, ET parameterization is preferred owing to the negligible mode II β function under low optical distortion. Because all skew quadrupoles are situated in the dispersion area, the vertical dispersion is not negligible and contributes to the vertical beam size, as shown in Formula 3.

$$\sigma_{x,y} = \sqrt{\beta_{x,y}\varepsilon_{x,y} + \sigma_\delta^2\eta_{x,y}^2} \tag{3}$$

In Fig. 2a and b, a comparison of the envelope method and Sands formalism for the beam-size computation of the 10% coupling setting demonstrates a good agreement between the two computation methods, and a significant vertical beam-size growth to approximately 7.5 μm, leading to an improvement in the Touschek lifetime. Figure 2b also shows that the vertical beam size is of the same order of magnitude as the horizontal beam size in a dispersion-free region.

With the same goal of quantifying the inevitable dispersion effect on the emittances, the effective emittance defined [39] by Formula 4 can be computed. Considering the brilliance, the effective emittance which represents the

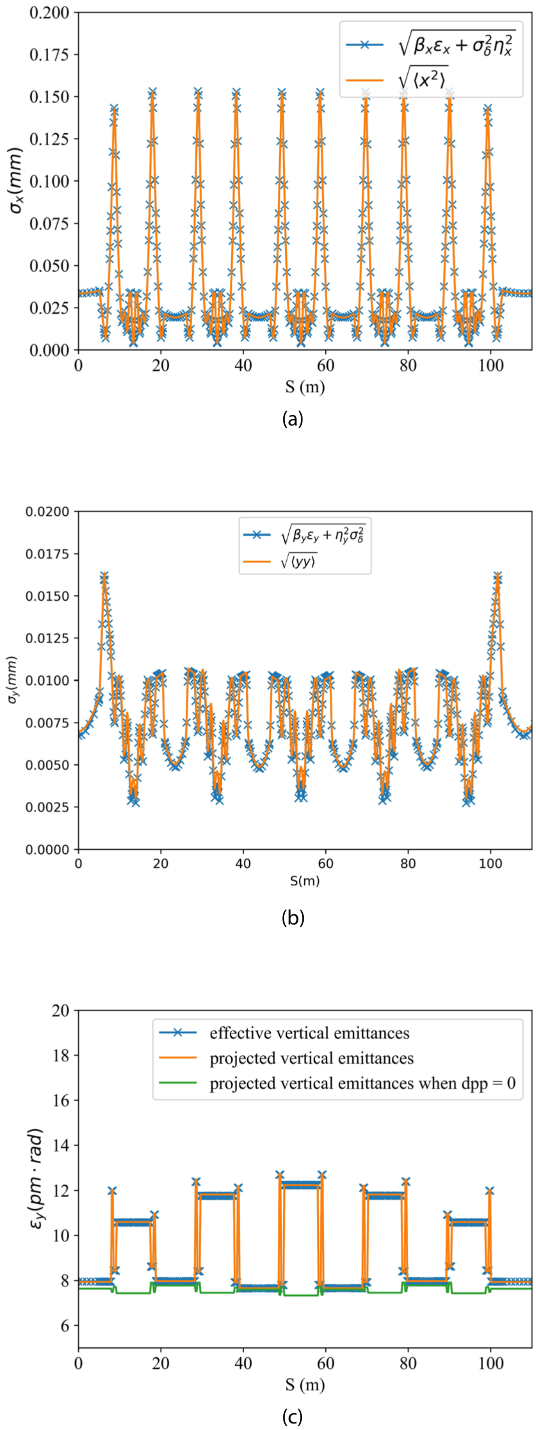

Fig. 2 (Color online) **a** and **b** Comparison of the envelope method and Sands formalism with ET parametrization for beam-size computation of the 10% coupling setting. **c** Comparison of the effective vertical emittances, projected vertical emittances, projected betatron emittance on the vertical axis when the energy spread and dispersion effect are ignored

total spread of circulating beams at a source point is a more crucial physical quantity. The vertical emittances from the contributions of the betatron coupling effect and vertical dispersion are also examined.

$$\begin{aligned}\epsilon_{x_{\text{eff}},y_{\text{eff}}}(s)) &= \sqrt{\epsilon_{x,y}^2 + \mathcal{H}_{x,y}(s)\epsilon_{x,y}\sigma_\delta^2}\\ \mathcal{H}_{x,y}(s) &= \beta_{x,y}(s)\eta_{x,y}'^2(s)\\ &\quad + 2\alpha_{x,y}(s)\eta_{x,y}(s)\eta_{x,y}'(s) + \gamma_{x,y}(s)\eta_{x,y}^2(s)\end{aligned} \tag{4}$$

Although the envelope method provides the projected emittances on the horizontal, vertical, and longitudinal axes whether or not the energy spread is present, the projected emittances vary along the storage ring and can be determined by the envelope matrix along the ring. Because there are beamlines using the bending magnet SR sources, the beam size and effective emittances in the arcs as well as the minimum brightness requirement must be considered and verified, respectively. Figure 2c shows that the results agree with the two methods and demonstrate the global dispersion effect on the vertical emittances in the matching section, which may cause an unwanted reduction in the brightness and other operational side effects.

Betatron coupling and vertical dispersion are simultaneously generated by the skew quadrupoles in the arc; therefore, it is difficult to suppress betatron coupling while maintaining the vertical dispersion, and vice versa, which may lead to significantly larger vertical emittances than expected in the arc. Therefore, the skew components in the dispersion-free region can be considered to solve this problem.

4 High betatron coupling with skew quadrupoles in dispersion-free region

4.1 Skew quadrupoles setting with optimization algorithm

For the ultra-low-emittance of fourth-generation synchrotron light sources, certain injection schemes have been proposed to match the significantly small dynamic aperture (DA), such as the swap-out injection, replacing the preceding pulsed-bump injection in third-generation light sources. The use of different injection schemes, divided into on-axis and off-axis injection, requires various storage ring performances and beam parameters. Off-axis injection, which requires a bumped orbit, is impossible with a strong betatron coupling of the horizontal and vertical planes as in a Mobius accelerator, whereas vertical dispersion can generate unwanted vertical emittances in the case of a large coupling ratio. Thus, a large coupling induced mainly by betatron coupling is necessary and worth further consideration.

Table 3 Optimization results of the NSGA-II algorithm for each emittance coupling ratio setting, calculated coupling ratio, calculated vertical emittances, and RMS beta-beating

Set $\varepsilon_y/\varepsilon_x$	$\varepsilon_{\mathrm{II}}/\varepsilon_{\mathrm{I}}$	$\varepsilon_{\mathrm{II}}$ (pm · rad)	β_x/β_y beating
0.10	0.1000	7.2	1.1%/0.8%
0.50	0.5001	28.6	5.1%/3.6%
1.00	1.0011	50.5	7.4%/6.6%

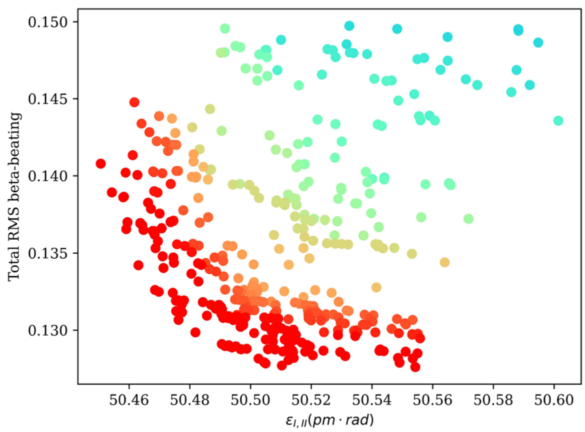

Fig. 3 (Color online) Optimization process for the 100% coupling set, objective functions: eigenemittances (horizontal axis) and RMS beta-beating (vertical axis); the points are colored according to their rank from blue to red

To prevent unwanted vertical dispersion, two additional skew quadrupoles (SQ family) were used in each straight section, as shown in Fig. 1, inspired by the generalization of the Mobius accelerator proposed by [13]. The skew quadrupoles with a length of 0.2 m were situated at the connection of the straight and matching sections to save the expensive space for insertion devices (Table 3).

All skew quadrupoles are powered independently; thus, 40 variables can be fed into the optimization algorithm. Instead of skew quadrupoles in the arc, emittances along the storage ring are well distributed if the beta function distortion is under control. The objective function and constrained condition retained the total eigenemittances, RMS beta-beating, and coupling ratio. We initialized a population of 100 children in the NSGA-II algorithm for optimization.

The results of the optimization demonstrate that a large coupling can still be achieved under a low beta function distortion, whereas full coupling is achievable under a relatively large beta function distortion. In the full-coupling case, the average value of the vertical dispersion is less than 10^{-4} m, which is negligible compared to that of the first scheme. The optimization process is illustrated in Fig. 3, which indicates that RMS beta-beating and eigenemittances can be simultaneously reduced with the diversity of the solutions, and finally converge. Because the transverse motion is coupled by skew quadrupoles, the transverse eigenemittances are equalized so as the radiation integrals and damping times, respectively, leading to an increase in the total emittances.

The bare SSRF-U lattice without the insertion devices has a natural emittance of $\varepsilon_x = 72.4\,\mathrm{pm \cdot rad}$, and the transverse damping partitions are $\mathcal{J}_x = 2.2675$ and $\mathcal{J}_y = 1$. With the exchange process of transverse motion, the damping partition is equalized as follows [40]: $\mathcal{J}_{\mathrm{I}} = \mathcal{J}_{\mathrm{II}} = (\mathcal{J}_x + \mathcal{J}_y)/2 = 1.6338$. Thus, emittances $\varepsilon_{\mathrm{I}} = \varepsilon_{\mathrm{II}} = \varepsilon_x/\left(1 + \frac{\mathcal{J}_y}{\mathcal{J}_x}\right) = 50.24\,\mathrm{pm \cdot rad}$, which demonstrates a good agreement of our optimization for minimizing the emittances. The total emittances can remain constant only when $\mathcal{J}_x = \mathcal{J}_y$; otherwise, brightness loss is inevitable in the round-beam scheme.

4.2 Equilibrium emittances based on tracking, global beam size, and effective emittances

The skew quadrupoles setting of 100% coupling was examined via tracking using the *Elegant* code. The tracking results show that both transverse beam distributions reach equilibrium, and that the horizontal and vertical emittances are equalized after 10,000 turns when reaching the equilibrium state with the predicted emittances and coupling ratio.

Because there was a relatively large optical distortion compared to that using the first skew quadrupole setting method, indicating that the mode II beta function was induced and needs to be computed, the Sands formalism using the ET parameterization may not be accurate as an approximation for computing the beam size. The Mais and Ripken (MR) parameterization [41] was applied in our computation as follows:

$$\sigma_{x,y} = \sqrt{\beta_{\mathrm{I},(x,y)}\varepsilon_{\mathrm{I}} + \beta_{\mathrm{II},(x,y)}\varepsilon_{\mathrm{II}} + \sigma_\delta^2\eta_{x,y}^2}. \quad (5)$$

As shown in Fig. 4a and b, the apparent vertical-size increase is almost entirely contributed to the betatron coupling, whereas the contribution of the local vertical energy oscillation $\eta_y\sigma_\delta$ is negligible. Here, the mode II Twiss parameter is given via MR parameterization.

Figure 4c demonstrates that the periodicity of the lattice is not broken under the 40 independent skew quadrupoles setting, and the three lines perfectly coincide with one another, indicating that there was no contribution of the vertical dispersion on this fully coupled lattice scheme. Therefore, compared to the dispersive coupled scheme, more uniform vertical emittances along the ring are obtained even when the energy spread is present.

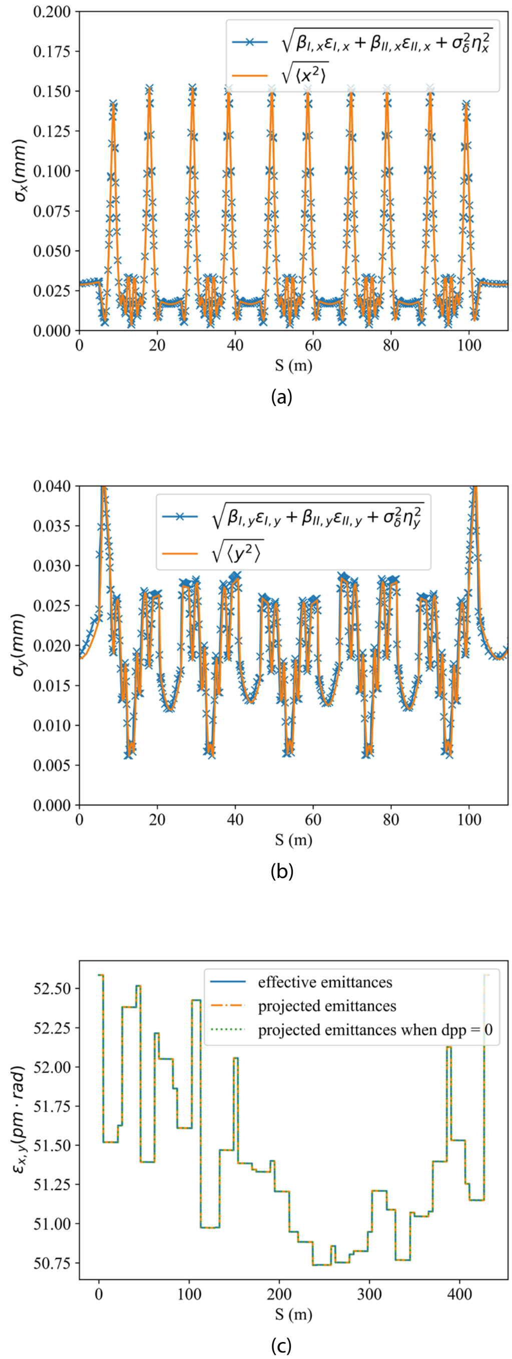

Fig. 4 (Color online) **a** and **b** Comparison of the envelope method and Sands formalism via MR parametrization for beam-size computation of the 100% coupling setting. **c** Comparison of the effective vertical emittances, projected vertical emittances, and projected betatron emittance on the vertical axis when the energy deviation and dispersion effect are ignored

5 Nonlinear effect and effect of lattice imperfections in strong coupled lattice

5.1 Dynamic aperture

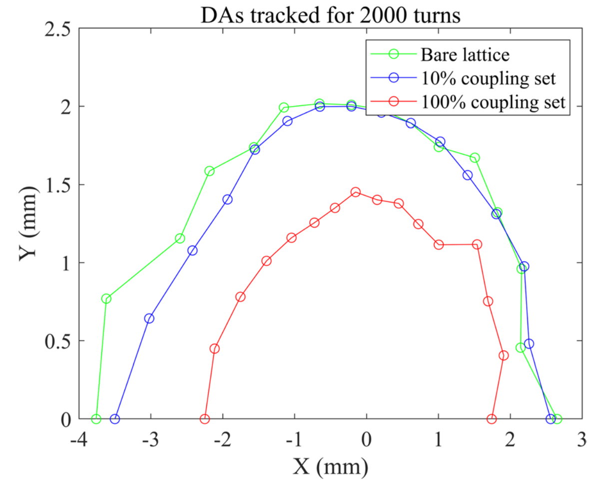

Fig. 5 (Color online) Dynamic aperture after correction of the chromaticities with two strong coupling setting schemes compared to original lattice

A sufficient dynamic aperture along with the injection and beam lifetime must be considered in the strong coupling lattice. The tracking results for checking the DA degradation are shown in Fig. 5. For the 10% coupling set, a slight reduction in DA after the linear chromaticities correction was observed compared to the bare lattice. For the 100% coupling set, the reduction in DA was apparent; however, it still reached a satisfactory value for the on-axis injection. The objective of the NSGA algorithm is to achieve a low RMS beta-beating of the coupled lattice because a large DA is expected to be maintained when the optical distortion is small. However, clear DA degradation was observed in the 100% coupling set, which indicates that a strong coupling effect may cause a nonlinear effect owing to the exchange of energy in the horizontal and vertical planes.

5.2 Energy acceptance

To study the effects that directly lead to beam-loss and therefore a reduced Touschek lifetime, the energy acceptance (EA) for each case of the coupling set was computed. The EA values for the two schemes and the design lattice are shown in Fig. 6a. Degradation of the EAs was observed for each case, especially for the 100% betatron coupling set, leading to a significant reduction in the Touschek lifetime, thus influencing our efforts in improving the beam lifetime by introducing a strongly coupled lattice in vain. The Betatron coupling motion exchanges particle motion in the transverse plane and may excite unwanted resonance and nonlinear effects. Octupoles can control the high-order chromaticity terms. With three families of octupoles in the dispersion region, the EA can be optimized by adjusting the position and strength of octupoles according to the

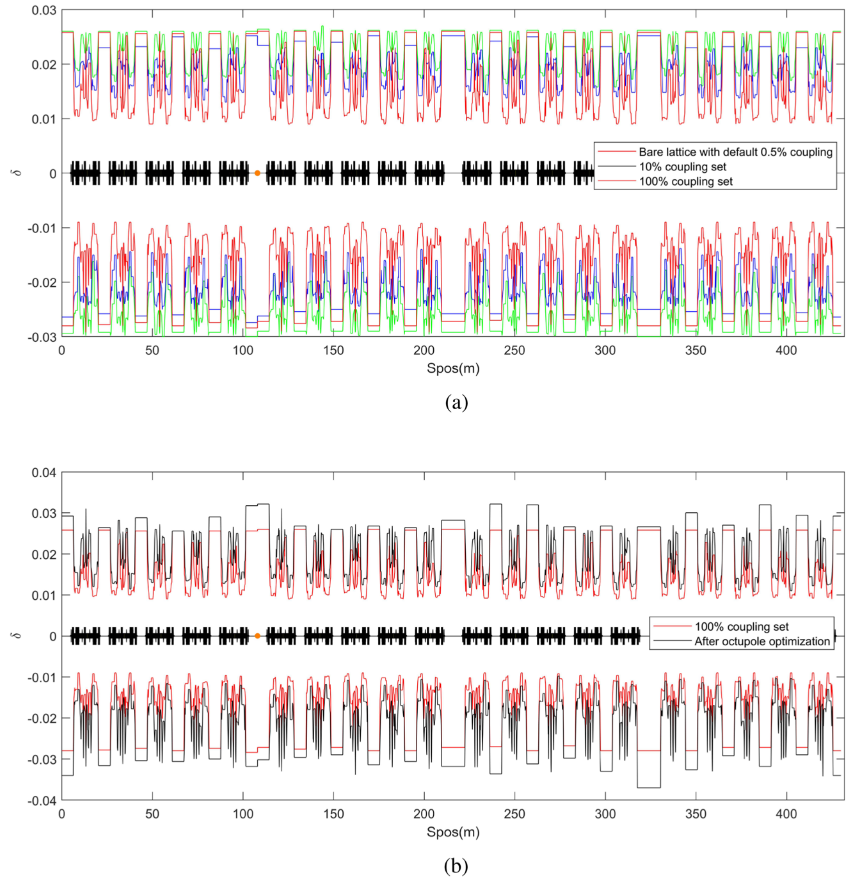

Fig. 6 (Color online) **a** Energy acceptance of the two strong coupling setting schemes compared to the original lattice; **b** energy acceptance of the 100% coupling set compared to the energy acceptance after octupole optimization

amplitude-dependent tune shift (ADTS). The preliminary optimization using the octupoles shown in Fig. 6b did not demonstrate a significant improvement in the low-energy acceptance region; however, an improvement in the global EA was observed.

5.3 Intra-beam scattering and beam lifetime

IBS and multiple small-angle Coulomb scattering events among the electrons in a bunch lead to electron diffusion in six-dimensional phase spaces. The *Elegant* code *IbsEmittance*, developed by implementing the Bjorken–Mtingwa model [39], was used to evaluate the influence of IBS. Based on the analysis of the Bjorken–Mtingwa model, we can conclude that reducing the density of electrons is an appropriate means of weakening the IBS effects. The total transverse emittances increased when the current increased, and the IBS effect of the high beam current was reduced in both coupling sets. Although both coupling schemes provided extra emittances, the total emittances were lower than those of the bare SSRF-U lattices when the beam current was relatively large, according to the calculation of the IBS effect.

Touschek scattering is large-angle Coulomb scattering between the electrons in a beam bunch that causes a momentum transport from the transverse motion to the longitudinal direction. In our case, the Touschek lifetime was calculated using the energy acceptance. Longitudinal stretching by a factor of five can be achieved with a harmonic cavity and applied in the computation of our beam lifetime. The beam lifetime was increased by a factor of 2–2.5 under a beam current of 500 ma with 500 bunches, ranging from 0.49 h for the bare lattice, 0.98 h for the 10% coupling set, and 1.21 h for the 100% coupling set, whereas lower total emittances owing to the suppression of the IBS effect in the high-current case and apparent degradation of the energy acceptance are demonstrated in the coupled schemes.

5.4 Effect of lattice imperfections

The error lattice was examined to estimate the performance of the global skew quadrupole setting under real-machine conditions. Focusing on the coupled elements, the roll errors on the quadrupoles and displacements of the sextupoles are applied in the error lattice. Fifty random-error seeds gradually increased from 500 μrad to 1000 μrad quadrupole roll errors, and the corresponding 500 μm to 1000 μm vertical offsets of the sextupoles were applied in the two schemes with different error strengths. Figure 7 demonstrates that the global skew quadrupoles setting can remain stable despite relatively large error seeds, proving the robustness of these

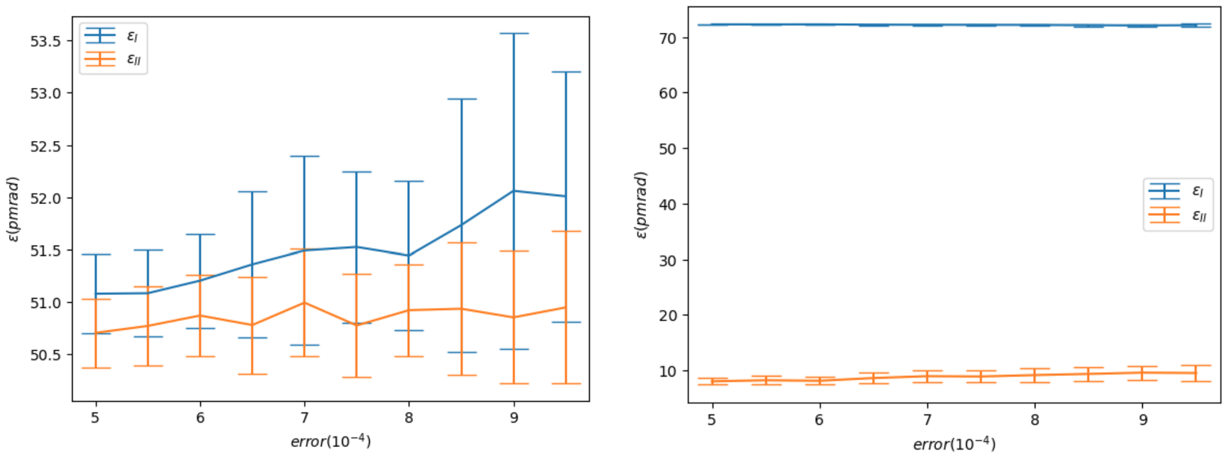

(a) (b)

Fig. 7 (Color online) Eigenemittance of the coupled lattice with imperfections. The error bar indicates a standard deviation of 50 random seeds. **a** 100% coupling set by betatron coupling; **b** 10% coupling set with vertical dispersion

schemes. On-resonance round-beam schemes always suffer from the challenge of a precise tune control, as well as an unstable beam size and emittances; conversely, this off-resonance scheme presents reduced complexity of the control and a more describable model for a detailed study.

6 Conclusion

Two off-resonance schemes utilizing a multi-objective optimization algorithm to achieve a large coupled lattice were investigated with a comprehensive analysis of the coupled lattice properties, such as the beam distribution and optics. The NSGA-II algorithm, owing to its flexibility in handling objective functions and constrained conditions, ensured minimal optical distortion and achieved the target coupling ratio.

The first scheme, with skew quadrupoles in the arc, simultaneously generates betatron coupling and vertical dispersion, which can generate additional vertical emittances especially when a large coupling ratio is required. Therefore, a coupling ratio near 10% was selected to reduce the increase in the emittance. The second scheme, which uses skew quadrupoles in the near-straight section, avoids unwanted vertical dispersion. Emittances can be equalized using bare betatron coupling. The simulation results and formula computations of the beam size and projected emittances were consistent with the optimization objectives. The dynamic aperture and energy acceptance were determined via tracking. The dynamic aperture was reduced in the full-coupling case; however, it still met the requirement for the on-axis injection. The degradation of the energy acceptance was apparent, and preliminary optimization using an octupole was applied to retain the beam lifetime. The IBS effect and Touschek lifetime were given for each case; an apparent reduction in the emittances induced by the IBS effect with a large beam current and an increase in the Touschek lifetime by factors ranging from 2 to 2.5 were achieved. The performance of a coupled lattice with imperfections was also examined. The off-resonance method was relatively more robust than the on-resonance method, which requires a dedicated tune feedback and monitoring system; however, the global setting of the strong-powered skew quadrupoles leads to inevitable total emittance growth. To achieve the target brightness, a dedicated lattice design for the reduction of the emittances and optimization of the damping partition is necessary.

Author Contributions All authors contributed to the study conception and design. Material preparation, data collection, and analysis were performed by Yi-Hao Gong, Shun-Qiang Tian, Xin-Zhong Liu, Shou-Zhi Xuan, Li-Yuan Tan, and Ling-Long Mao. The first draft of the manuscript was written by Yi-Hao Gong, and all authors commented on previous versions of the manuscript. All authors read and approved the final manuscript.

Data Availability Statement The data that support the findings of this study are openly available in Science Data Bank at https://cstr.cn/31253.11.sciencedb.j00186.00147 and https://www.doi.org/10.57760/sciencedb.j00186.00147.

Declaration

Conflict of interest The authors declare that they have no conflict of interest.

References

1. P. Tavares, E. Al-Dmour, Å. Andersson et al., Commissioning and first-year operational results of MAXIV 3 GeV ring. J. Synch. Rad. **25**, 1291–1316 (2018). https://doi.org/10.1107/S1600577518008111

2. P. Raimondi, N. Carmignani, L.R. Carver et al., Commissioning of the hybrid multibend achromat lattice at the European Synchrotron Radiation Facility. Phys. Rev. Accel. Beams **24**, 110701 (2021). https://doi.org/10.1103/PhysRevAccelBeams.24.110701
3. L. Liu, M. B. Alves, F. H. de Sá et al., Status of sirius operation. *JACoW. IPAC2022*:TUPOMS002 (2022). https://doi.org/10.18429/JACoW-IPAC2022-TUPOMS00
4. Y. Jiao, G. Xu, X.H. Cui et al., The HEPS project. J. Sync. Rad. **25**, 1611 (2018). https://doi.org/10.1107/S1600577518012110
5. Y. Sun, M. Borland, Alternate lattice design for advanced photon source multi-bend achromat upgrade. in *Proceedings of IPAC2015*, Richmond, VA, USA, 3–8 May (2015). https://doi.org/10.18429/JACoW-IPAC2015-TUPJE071
6. C. Steier, A. Allézy, A. Anders et al., Status of the conceptual design of ALS-U. in *Proceeedings of the 9th International Particle Accelerator Conference* Vancouver, BC, Canada, April 29–May 4, (2018). https://doi.org/10.18429/JACoW-IPAC2018-THPMF036
7. J. Xu, Z. Ren, P. Yang et al., A seven-bend-achromat lattice option for the HALF storage ring. J. Instrum. **17**, P01001 (2022). https://doi.org/10.1088/1748-0221/17/01/P01001
8. P.H. Yang, G.W. Liu, J.H. Xu et al., Design and comparison of hybrid multi-bend achromat lattices for HALF storage ring. Nucl. Sci. Tech. **34**, 107 (2023). https://doi.org/10.1007/s41365-023-01252-w
9. P. Klysubun, T. Pulampong, P. Sudmuang. Design and optimization of SPS-II storage ring. in *Proceedings of IPAC2017*. https://accelconf.web.cern.ch/ipac2017/papers/wepab086.pdf
10. E. Karantzoulis, Elettra 2.0 - The diffraction limited successor of Elettra. Nucl. Inst. Meth. A **880**, 158–165 (2018). https://doi.org/10.1016/j.nima.2017.09.057
11. X.Z. Liu, S.Q. Tian, X. Wu et al., Intra-beam scattering and beam lifetime in a candidate lattice of the soft X-ray diffraction-limited storage ring for the upgraded SSRF. Nucl. Sci. Tech. **32**, 83 (2021). https://doi.org/10.1007/s41365-021-00913-y
12. A. Piwinski, The touschek effect in strong focusing storage rings. arXiv:physics/9903034 [physics.acc-ph] (1999). https://arxiv.org/abs/physics/9903034
13. M. Aiba, M. Ehrlichman, A. Streun, Round beam operation in electron storage rings and generalization of mobius accelerator. in *IPAC'15*, Richmond, VA, USA, May 3–8 (2015). https://doi.org/10.18429/JACoW-IPAC2015-TUPJE045
14. X. Huang, An ultimate storage ring lattice with vertical emittance generated by damping wigglers. Nucl. Inst. Meth. A. **777**, 118–122 (2015). https://doi.org/10.1016/j.nima.2014.12.097
15. X.Z. Liu, S.Q. Tian, L.Y. Tan et al., Applications of vertical damping wigglers in an x-ray diffraction limited storage ring. Nucl. Inst. Meth. A **1056**, 168653 (2023). https://doi.org/10.1016/j.nima.2023.168653
16. R. Talman, A proposed mobius accelerator. Phys. Rev. Lett. **74**, 1590 (1995). https://doi.org/10.1103/PhysRevLett.74.1590
17. A. Franchi, E. Mtral, R. Toms, Emittance sharing and exchange driven by linear betatron coupling in circular accelerators. Phys. Rev. ST Accel. Beams **10**, 064003 (2007). https://doi.org/10.1103/PhysRevSTAB.10.064003
18. C. Du, J. Wang, D. Ji et al., Studies of round beam at heps storage ring by driving linear difference coupling resonance. Nucl. Inst. Meth. A **976**, 164264 (2020). https://doi.org/10.1016/j.nima.2020.164264
19. K. Deb, A. Pratap, S. Agarwal et al., A fast and elitist multiobjective genetic algorithm: NSGA-II. IEEE Trans. Evol. Comput. **6**, 182 (2002). https://doi.org/10.1109/4235.996017
20. K. Ohmi, K. Hirata, K. Oide, From the beam-envelope matrix to synchrotron-radiation integrals. Phys. Rev. E **49**, 751 (1994). https://doi.org/10.1103/PhysRevE.49.751
21. M.Z. Zhang, S.Q. Tian, K. Wang et al., Study of new injection schemes for the SSRF storage ring. Nucl. Tech. **40**, 110101 (2017). https://doi.org/10.11889/j.0253-3219.2017.hjs.40.110101 (in Chinese)
22. Y.Y. Wang, L. Shang, F.L. Shang et al., Simulation of storage ring injection of HLS II. Nucl. Sci. Tech. **27**, 2 (2016). https://doi.org/10.1007/s41365-016-0007-8
23. X. Wu, S.Q. Tian, X.Z. Liu et al., Designand commissioning of the new ssrf storage ring lattice with asymmetric optics. Nucl. Inst. Meth. A **1025**, 166098 (2022). https://doi.org/10.1016/j.nima.2021.166098
24. H.J. Xu, Z.T. Zhao, Status and progress of SSRF project. Nucl. Sci. Tech. **19**, 1–6 (2008). https://doi.org/10.1016/S1001-8042(08)60013-5
25. S.Q. Tian, B.C. Jiang, Q.G. Zhou et al., Lattice design and optimization of the SSRF storage ring with super-bends. Nucl. Sci. Technol. **25**, 010102 (2014). https://doi.org/10.13538/j.1001-8042/nst.25.010102
26. X.Z. Liu, S.Q. Tian, X. Wu et al., Feedforward compensation of the insertion devices effects in the SSRF storage ring. Nucl. Sci. Tech. **33**, 70 (2022). https://doi.org/10.1007/s41365-022-01052-8
27. C.L. Li, S.Q. Tian, W.Z. Zhang, Study on the vertical emittance for the SSRF Phase II project. Nucl. Tech. **39**, 050102 (2016) https://doi.org/10.11889/j.0253-3219.2016.hjs.39.050102 (in Chinese)
28. X. Wang, S.Q. Tian, G.M. Liu, Low-alpha optics design for SSRF. Nucl. Sci. Technol. **21**, 134–140 (2010). https://doi.org/10.13538/j.1001-8042/nst.21.134-140
29. S.Q. Tian, B.C. Jiang, Y.B. Leng et al., Double mini betay optics design in the SSRF storage ring. Nucl. Sci. Tech. **25**, 030101 (2014). https://doi.org/10.13538/j.1001-8042/nst.25.030101.
30. Y. Li, R. Rainer, Designing linear lattices for round beam in electron storage rings using the solution by linear matrices analysis. Phys. Rev. Accel. Beams **25**, 040702 (2022). https://doi.org/10.1103/PhysRevAccelBeams.25.040702
31. A. Wolski, Low-emittance storage rings. arXiv:1507.02213 [Physics], 2015. https://doi.org/10.5170/CERN-2014-009.245
32. A. Terebilo, Accelerator toolbox for MATLAB. Tech. Rep. SLAC-PUB- **8732**, 784910 (2001). https://doi.org/10.2172/784910
33. M. Borland, ELEGANT: A flexible SDDS-compliant code for accelerator simulation. Tech. Rep. **LS-287**, 761286 (2000).https://doi.org/10.2172/761286
34. X. Huang, J. Safranek, Nonlinear dynamics optimization with particle swarm and genetic algorithms for spear3 emittance upgrade. Nucl. Inst. Meth. A **757**, 48 (2014). https://doi.org/10.1016/j.nima.2014.04.078
35. S. Tian, A design strategy of achievable linear optics for a complex storage ring lattice. Chin. Phys. C **34**, 1009 (2010). https://doi.org/10.1088/1674-1137/34/7/015
36. D.A. Edwards, L.C. Teng, Parametrization of linear coupled motion in periodic systems. IEEE Trans. Nucl. Sci. **20**, 885 (1973). https://doi.org/10.1109/TNS.1973.4327279
37. M. Sands, Physics of electron storage rings: An introduction. United States: N. p. (1970). https://doi.org/10.2172/4064201
38. D. Sagan, D. Rubin, Linear analysis of coupled lattices. Phys. Rev. ST Accel. Beams **2**, 074001 (1999). https://doi.org/10.1103/PhysRevSTAB.2.074001
39. H. Tanaka, A. Ando, Minimum effective emittance in synchrotron radiation sources composed of modified chasman green lattice. Nucl. Inst. Meth. A **369**, 312 (1996). https://doi.org/10.1016/0168-9002(95)00773-3
40. V. Ziemann, A. Streun, Equilibrium parameters in coupled storage ring lattices and practical applications. Phys. Rev. Accel. Beams **25**, 050703 (2022). https://doi.org/10.1103/PhysRevAccelBeams.25.050703

41. I. Borchardt, E. Karantzoulis, H. Mais et al., Calculation of beam envelopes in storage rings and transport systems in the presence of transverse space charge effects and coupling. Z. Phys. C **39**, 339–349 (1988). https://doi.org/10.1007/BF01548283
42. S.K. Tian, J.Q. Wang, G. Xu et al., Intra-beam scattering studies for low emittance at baps. Chin. Phys. C **39**, 067001 (2015). https://doi.org/10.1088/1674-1137/39/6/067001